PHYSICAL REVIEW B **83**, 214415 (2011)

Impact of local lattice distortions on the structural stability of Fe-Pd magnetic shape-memory alloys

Markus E. Gruner* and Peter Entel

Faculty of Physics and Center for Nanointegration, CeNIDE, University of Duisburg-Essen, D-47048 Duisburg, Germany

(Received 11 March 2011; revised manuscript received 12 May 2011; published 14 June 2011)

The binding surface of Fe-rich Fe-Pd alloys is explored by means of first-principles calculations in the framework of density functional theory involving unconstrained optimization of the atomic positions within a 108-atom supercell. We find that static displacements arising from geometric optimization provide an important contribution to the total energy, effectively compensating favorable contributions gained from introducing $L1_2$ order in stoichiometric Fe_3Pd. In the concentration range for magnetic shape-memory applications, the energy profile with respect to tetragonal distortion is altered qualitatively, shifting the ground state of the intermixed disordered system from face-centered cubic (fcc) to body-centered tetragonal (bct). From the radial pair distribution function and electronic density of states obtained from a 500-atom supercell calculation we identify the origin of the displacements. These arise from the size-dependent relaxations of the larger Pd atoms, on the fcc side in combination with a Jahn-Teller-like rearrangement of Fe d states at the Fermi level.

DOI: 10.1103/PhysRevB.83.214415 PACS number(s): 75.50.Bb, 81.30.Kf, 71.55.Jv, 71.15.Mb

I. INTRODUCTION

In recent time, materials exhibiting magnetic shape-memory (MSM) behavior have become the subject of intense research (for a recent overview on this topic, see Refs. 1–3 and references therein). In MSM materials, large mechanical strains of several percent can be induced by reasonable magnetic fields of the order of one Tesla. This entitles them for usage in alternative sensor or actuator systems. The prevailing mechanism relies on the easy reorientation of structural (martensitic) domains, which are coupled to the direction of magnetization by the large magnetocrystalline anisotropy of the material. For applications with mass market potential, systematic improvements of the existing MSM materials need to be realized. These include a larger operating range up to temperatures around 100 °C, for example, for applications in the automotive sector as well as better mechanical properties for postprocessing.

An important group of MSM alloys are Fe-based alloys with Pt-group elements with compositions allowing a face-centered cubic (fcc)–body-centered cubic (bcc) transformation in the respective temperature range. Bulk iron undergoes a structural phase transformation around 1185 K from a fcc high-temperature phase to a low-temperature bcc phase, which is ferromagnetic with a Curie temperature of 1043 K. Increasing the valence electron concentration e/a through alloying elements with a larger number of d electrons systematically decreases the structural transition temperature. The structural transition is displacive and diffusionless; it occurs between a high-temperature high-symmetry phase called austenite and a low-temperature phase, called martensite, in which the symmetry is usually lowered, for example, by tetragonal distortions. In ferromagnetic Fe-based alloys with e/a between 8.7 and 8.5, the martensitic transition disappears and fcc austenite becomes the stable ground-state structure (see, e.g., Refs. 4–6 for an introduction).

Iron alloys with Pt-group elements are known for a variety of anomalies with respect to their magnetostructural properties. Some of them, as the systematic reduction of thermal expansion termed the Invar effect, and the above-mentioned magnetic shape-memory behavior are of high technological importance. The Invar effect is especially pronounced in $Fe_{65}Ni_{35}$, $Fe_{70}Pd_{30}$, and $Fe_{72}Pt_{28}$ alloy compositions and has been under intense scrutiny for more than a century.[7–9] In the past three decades, the MSM properties of Fe-based alloys also moved into the focus of scientific interest.[10–12] Fe-based systems with significant MSM behavior are based on disordered $Fe_{70}Pd_{30}$ alloys, highly ordered Fe_3Pt, and also Fe-Ni-Co alloys with an addition of a few at-% Ti.[13–16] However, the considerable magnetic-field-induced strain (MFIS) observed in the former two, 3.0 % for Fe-Pd and 2.3% for Fe_3Pt, are reported for prohibitively low temperatures of 77 K and 4 K, respectively. At temperatures approaching the austenitic phase, the MFIS is decreasing as does also the c/a ratio, which determines the upper limit of the achievable strain. Current strategies to shift the martensitic temperature to a relevant range involve the co-alloying with a third element. The most promising candidates in this respect found so far are Mn and Cu.[17–20]

In the Fe-based alloys, the MSM effect is not as pronounced as for the prototype Ni-based Heusler alloys like Ni_2MnGa,[21–23] but it is natural to assume its origin to be related. One common key ingredient in the Heusler systems is the appearance of modulated martensites[24–26] while it is a slightly distorted face-centered tetragonal (fct) phase in the case of Fe-Pt and Fe-Pd. The fct phase appears as an intermediate structure between the high symmetry austenite and the low-temperature martensite, which is body-centered tetragonal in the case of the ferrous alloys.[10–12]

A helpful parametrization of the martensitic transformation process is established by the so-called Bain path.[27] It relates the martensite and austenite in terms of the tetragonal distortion c/a. Since both ends can have cubic symmetry (i.e., fcc and bcc as in the case of Fe), there is some ambiguity in the description. In the present work, we chose the austenite as a reference, thus $c/a = 1$ for fcc and $c/a = \sqrt{1/2}$ for bcc. Recently, a number of independent investigations were addressing the structural stability of the ordered Fe-rich phases with Pt-group

elements with respect to tetragonal distortions along the Bain path.[28–30] Together with previous studies, predominately touching magnetic properties, electronic structure,[31–35] and Invar-related anomalies,[36–41] many features of these alloys can now be regarded as reasonably well understood. However, the ordered MSM alloy Fe_3Pt is—because of its extremely low martensite temperature—an interesting candidate from the fundamental point of view, but not a prospective basis for the development of real-world actuators or sensors. Furthermore, the qualitative differences in the binding surface, that is, the total energy $E(V,c/a)$ as a function of volume V and tetragonal distortion c/a, with respect to different realizations of order show that the ordered models are only of restricted use to estimate structural properties of disordered Fe alloys with Pt-group elements. Therefore explicit modeling of a statistically random arrangement of atoms is inevitable for a deeper understanding of the instabilities leading to the MSM behavior in the disordered candidates.

For the description of disorder, essentially two popular strategies exist. The first and apparently more elegant way is to model disorder analytically by effectively mixing the electronic description of the atoms on the corresponding lattice sites (for a recent review on this topic, see Ref. 42). This allows one still to make use of Bloch's theorem and describe the structure in small (even primitive) lattice cells, while translational symmetry is strictly speaking absent in the disordered case. This can be done by the so-called virtual crystal approximation (VCA) which relies on a superposition of the potentials to solve the electronic problem. A related approach is the coherent potential approximation (CPA). Here, in contrast, not the potential, but the scattering properties of the different atoms are superimposed, which are represented by the scattering path operators belonging to the atoms of a given species. In order to describe a random medium, these atoms are thought to be embedded into an effective medium as an impurity. This impurity problem is conveniently solved in terms of Green's functions, which can be used to determine the coherent scattering path operator of the effective medium in an additional self-consistency cycle. Thus, CPA implementations are frequently (but not exclusively) found in connection with Korringa-Kohn-Rostoker Green's function methods.

The second route relies on a straightforward explicit description of disorder using as-large-as-possible supercells. Their sites are then randomly occupied by "pure" atoms according to a predefined composition (and distribution). Apart from finite size effects, which are related to the inherent inability to correctly reproduce correlations with distances larger than the extension of the supercell, a truly random distribution is only obtained in the limit of large numbers (i.e., as the average of a large number of supercells generated in this way). For each single configuration, statistical fluctuations within the distributions might lead to deviations in the measured properties from the envisaged statistical average values. In order to take care of the fact that in Fe-based MSM alloys the relevant phase is only observed in a concentration window of a few atomic percent, supercell sizes in the order of 100 atoms have to be considered. For such large systems, systematic averaging over dozens of configurations calculated within DFT is prohibitive, if at the same time the evolution of the properties upon variation of an external parameter (e.g., the tetragonal distortion) is to be monitored. A bypass to this problem provides the generation of so-called special quasirandom structures[43] (SQS) allowing an optimized representation of statistical disorder within small unit cells. Here, the configurations are actively selected according to their compliance to a given statistical distribution, which is described in terms of pair (and triplet) correlation functions. Reproducing the statistical distribution of atoms and retaining a small supercell are mutually exclusive conditions, which might be optimized potentially at the expense of other properties. Nevertheless, for several problems, it has been proven a suitable compromise allowing for fairly small supercells.[44–48]

From the theoretical side the existence of the fct intermediate phase in Fe-Pd alloys was addressed so far in the framework of density functional theory electronic structure calculations in combination with an analytic description of disorder in terms of the CPA. Initial work was performed by Stern *et al.*[49,50] using the KKR Green's function method. An extensive survey of the compositional dependence of structural and magnetic properties of Fe_xPd_{1-x} alloys on the basis of the linearized muffin-tin orbitals method (LMTO) in connection with the CPA was recently published by Burzo and Vlaic.[51] A major advance concerning understanding of the involved electronic mechanism has been gained by the work of Ingo Opahle and coworkers.[52] Unlike the other groups, the authors use the CPA in connection with the full potential localized orbital method (FPLO),[53–55] which is expected to yield comparable accuracy to full potential plain wave methods. Opahle *et al.* propose that, in analogy to the Ni-Mn-Ga Heusler alloys, a band-Jahn-Teller mechanism is responsible for the occurrence of the thermoelastic transition from the fcc to the fct phase. The transition is driven by the degeneracy of the minority channel Fe-d states with t_{2g} symmetry at the Fermi level close to the Γ point, which is split in the martensitic phase, thereby lowering the band energy. The minority spin density of states corresponding to the cubic (fcc) and tetragonal (fct) structure verify a shift of Fe d states away from the Fermi level. The authors argue that the resulting gain in band energy of about 14 meV can lead to the formation of a local minimum corresponding to a new, metastable phase—presupposed that the binding surface $E(V,c/a)$ is sufficiently flat with respect to c/a, as it may be expected close to the martensitic fcc-bct transition. Indeed the authors observe a flattened energy landscape for a system with 80 at-% Fe. This is consistent with the experimental observation that $Fe_{70}Pd_{30}$ thin films can be grown epitaxially on various substrates, thereby inducing tetragonal distortions which span nearly the complete Bain path.[56] The shift in composition is a consequence of the use of the local spin density approximation for the exchange-correlation functional in this work. The calculated binding curve $E(c/a)|_{V=\text{const}}$ exhibits an additional shallow minimum around $c/a = 0.88$ which might be attributed to the fct phase.

On the other hand, it has been shown recently by first-principles calculations that the phase stability of the corresponding ordered MSM alloys is influenced by a characteristic atomic shuffle which is indicated as a soft mode in the phonon dispersion relations. In $L1_2$ ordered stoichiometric alloys Fe_3Pt, Fe_3Pd and Fe_3Ni imaginary contributions appear in one acoustic branch at the M point,[30] which indicates the

instability of the $L1_2$ lattice. This can be resolved by suitable displacements of the Fe atoms made in a $2 \times 2 \times 1$ supercell according to the eigenvectors of the unstable phonon mode, which is accompanied by a reduction of the initially cubic symmetry to a tetragonal one. The origin of this instability has again been traced back to an accumulation of Fe states at the Fermi surface which are redistributed by the corresponding lattice relaxation.

The purpose of the present investigation is therefore to explore the influence of local lattice distortions on the binding surface of disordered Fe-based MSM alloys. We will compare the binding surface $E(c/a, V)$ or, respectively, constant volume cross sections of it, for ordered and disordered configurations for different compositions in the MSM region. The latter are optionally allowed to undergo relaxations according to the interatomic forces. Naturally, this implies the use of supercells instead of the CPA. An important difficulty with respect to our goal arises from the fact that the randomized distribution of atoms in the supercell breaks a given—in this case, cubic—symmetry of the supercell. This is especially severe in the case of small cells, while in the limit of large numbers these effects are averaged out. Thus, if in finite cells, structural energies (or other properties) are calculated as a function of the symmetry breaking tetragonal distortion, the results will in general differ according to in which of the initially equivalent cubic directions the distortion was applied. Using small cells containing only a few dozens of atoms, this might lead to significant errors. Therefore, the authors decided to employ considerably larger cells consisting of at least 108 atoms. The improved statistical basis also reduces the necessity to optimize the arrangement of the elements with respect to the correlation function thereby avoiding possible unwanted side effects on other properties. Starting from a purely (uncorrelated) random distribution of atoms, the obtained configuration subsequently underwent several tests in order to exclude that an—unlikely, but possible—pathological distribution of atoms may lead to obviously artificial results.

II. COMPUTATIONAL DETAILS

The supercell calculations were carried out in the framework of the density functional theory[58] taking advantage of the Vienna *ab-initio* simulation package (VASP),[59] which is efficiently parallelized allowing for the treatment of large supercells on massively parallel computer hardware.[60] VASP achieves an excellent compromise between speed and accuracy by describing the wave functions of the valence electrons using a plane wave basis set while taking advantage of the projector augmented wave (PAW) approach,[61] which takes care of the interaction with the core electrons. For the accurate description of structural properties of ferrous alloys, the use of the generalized gradient approximation (GGA) for the representation of the exchange-correlation functional is desirable. As in our previous *ab initio* study for ordered Fe_3Pd we used the formulation of Perdew and Wang[62,63] in connection with the spin interpolation formula of Vosko *et al.*[64]

For systems of the order of 10^2 atoms the computational demands of DFT calculations also require compromises with respect to the technical parameters limiting the accuracy, for example, in terms of a reduced set of electrons treated as valence electrons or a limited k mesh. In the present case, we used potentials explicitly describing the $3d^7 4s^1$ electrons for Fe and $4d^9 5s^1$ for Pd in combination with an energy cutoff of $E_{\text{cut}} = 335$ eV. Thus, the first effort should be dedicated to a comparison to well-known results obtained with high accuracy. The optimum benchmark to estimate possible errors made in calculations of real Fe-Pd MSM systems offers the ordered Fe_3Pd alloy. Following this line of thought, the investigations of the binding surfaces were started by using as a model system the 108-atom supercell (i.e., $3\times3\times3$ $L1_2$ simple cubic primitive cells containing four atoms each). For comparison, the Brillouin zone (BZ) was integrated in reciprocal space over two Monkhorst-Pack[65] meshes with $2\times2\times2$ and $4\times4\times4$ k points in the full BZ, respectively. In both cases BZ integration was carried out with the finite temperature smearing according to Methfessel and Paxton[66] with a broadening of $\sigma = 0.2$ eV. The final comparison to previous benchmark results[30] obtained with different codes and exchange correlation potentials is shown in Fig. 1. The supercell calculations with k mesh of $4\times4\times4$ reproduce the corresponding primitive cell results with a (relative) deviation of the order of 1 meV/atom. With the smaller k mesh, the accumulated energy difference along the Bain path amounts to 6–8 meV/atom. Keeping in mind that these calculations are faster by a factor of eight, this can still be regarded a reasonable compromise for many cases

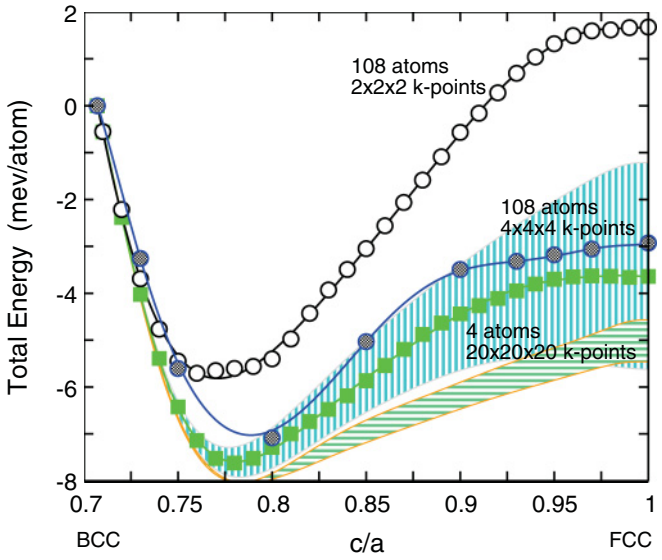

FIG. 1. (Color online) Benchmark calculations for ordered Fe_3Pd with tetragonal distortion along the Bain path ranging from bcc to fcc showing a comparison of the total energy obtained within the primitive cell (four atoms) and large k-point set, and a supercell ($3\times3\times3$ primitive cells) with different k meshes. A constant volume of 13.08 Å^3/atom is assumed. For all curves, the energy is related to the bcc state, $c/a = \sqrt{0.5}$, as a reference. The hatched areas refer to results obtained using the full potential linearized augmented plane wave method (FLAPW) implemented within the WIEN2K package [57] (horizontal lines) and VASP results obtained with different PAW potentials and varying formulations of the GGA exchange correlation potential (vertical lines). Details can be found in Ref. 30. Supercell calculations with a k mesh of $4\times4\times4$ reproduce the benchmark results with reasonable accuracy of a few meV/atom along the full Bain path.

(e.g., where the corrugation of the energy profile significantly exceeds this error), or for a comparison of energies obtained with the constraint of a fixed cell shape, as the requirements for convergence with respect to the k mesh can be somewhat relaxed here.

The investigation of the disordered structures took place using an analogous $3\times3\times3$ supercell containing simple cubic (sc) elements with four atoms each (108 atoms in total). The atoms were distributed randomly over the sites. The binding surface was determined in a two-step fashion. First, for each tetragonal distortion, the internal degrees of freedom were optimized according to the interatomic forces with the built-in conjugate gradient scheme using the smaller $2\times2\times2$ Monkhorst-Pack grid. The interatomic forces were converged down to a maximum value of 20 meV/Å, while the conversion criterion for the energies assured a numerical accuracy of 10^{-4} eV of each ionic step. The Bain path was sampled consecutively starting from $c/a = 1.0$ (fcc) using the fully relaxed positions of the previously obtained run for the next larger c/a value as a starting point for the new structure. The second step consists in a single point calculation on the denser $4\times4\times4$ grid without further relaxation, in order to allow for a sufficient accuracy for the comparison of the energies between the different cell shapes. For the accurate determination of the radial distribution function and the electronic density of states (DOS), a 500-atom supercell was set up ($5\times5\times5$ simple cubic cells with four atoms each). The structural optimization again took place on a $2\times2\times2$ Monkhorst-Pack grid in the fashion described above, while the DOS was evaluated in another single-step calculation with a $4\times4\times4$ Monkhorst-Pack grid and integration over the BZ took place using the tetrahedron method with Blöchl corrections.[67] The precision of the electronic self-consistency cycle was increased to 10^{-6} eV here.

For comparative purposes, additional calculations have been carried out with a KKR-CPA approach implemented in the Munich SPR-KKR code[68,69] (version 5.4) using either a four-atom cell describing the $L1_2$ type of order and correspondingly applied tetragonal distortion (space group number 123, I4/mmm) or the same cell with complete disorder on all positions. The muffin-tin radii were kept consistent (same for all positions) in both setups. We used a $15\times15\times15$ k mesh (288 points in the irreducible BZ). Angular momentum expansion was taking place up to f states and 30 points were used to describe energy contour in the complex plane. The calculations were carried out within the atomic sphere approximation (ASA) as well as in full potential mode, both in combination with the GGA exchange-correlation functional of Perdew, Burke, and Ernzerhof[70] The SPR-KKR calculations have been performed in the fully relativistic mode, whereas, in contrast, for the VASP calculations a scalar relativistic description of the Hamiltonian has been used throughout.

III. ORDER AND STATIC DISPLACEMENTS IN $Fe_{75}Pd_{25}$ ALLOYS

As indicated above, generating a single cell with 108 randomly chosen atoms may in general not be sufficient to guarantee a perfect statistical distribution. In the present case, the fraction of Pd-Pd, Fe-Pd, and Fe-Fe nearest neighbor pairs in the sample served as a measure. For the $Fe_{75}Pd_{25}$ configuration to be used in the further course of this study, values of 6.33%, 56.33%, and 37.35% were found for the three possibilities, respectively, which agrees well with the values of a perfectly random distribution, which are 6.25%, 56.25%, and 37.5%, respectively. Similar agreement was also reached with respect to the fraction of next-nearest and third-nearest neighbor pairs. A further, more pragmatic verification can be obtained from the comparison of the ordering energy ΔE_{order} along the whole Bain path with the results of an analytical description of disorder within the KKR-CPA scheme (c.f. Fig. 2). The ordering energy is defined as the difference $\Delta E_{\text{order}}(c/a) = E_{\text{disordered}}(c/a) - E_{L1_2}(c/a)$ between the disordered and the $L1_2$ ordered configuration. In both cases, the atoms were placed on ideal lattice positions as the KKR-CPA scheme does not allow for geometrical optimization. For all c/a ratios, the values obtained with the supercell approach lie in a distance of a few meV/atom to both KKR-CPA results, confirming that a representative distribution of the atomic species on the supercell sites was chosen for this comparison.

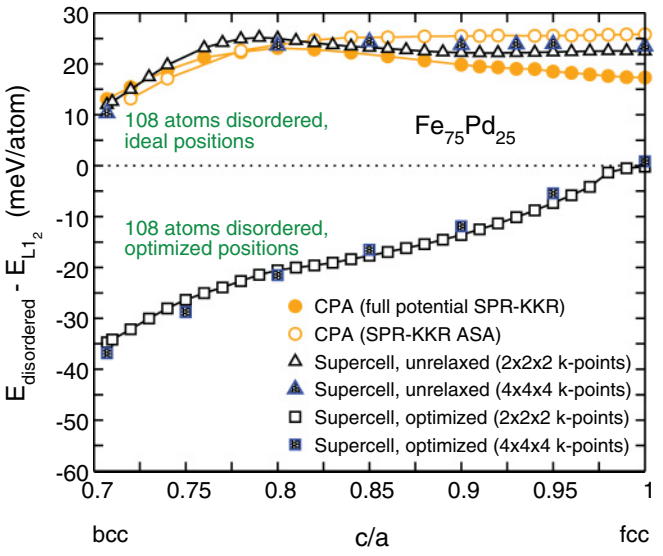

FIG. 2. (Color online) Comparison of the (relative) ordering energies $\Delta E_{\text{order}} = E_{\text{disordered}} - E_{L1_2}$ between KKR-CPA calculations (circles) and plane wave supercell calculations (triangles and squares). Static relaxations (squares) lead to a significant lowering of the energy of the disordered system, which is nonuniform along the Bain path. Without taking into account atomic relaxations (triangles), the explicit supercell description of disorder agrees well with the CPA results.

All calculations consistently suggest a positive ΔE_{order}, which at first sight implies that the $L1_2$-type order should be preferred for fcc and bcc structures and, correspondingly, all tetragonal structures in between. However, this outcome changes completely if the atoms in the supercell are allowed to adjust their positions according to the interatomic forces. Now the energy of the disordered structure becomes at par with the perfectly $L1_2$ ordered one at the fcc end and slips about 35 meV/atom below it on the bcc side. On the other hand, condensation of the imaginary phonon mode at the M point leads to a further gain in the order 5 meV/atom for the

$L1_2$ ordered arrangement in a face-centered environment (not included in Fig. 2).[30] Nevertheless, since the disordered alloy benefits from configurational entropy, it appears unlikely that a considerable degree of long-range order might be achieved in the thermodynamic limit, since the main thermodynamic driving force working in favor of the ordered structures is nearly absent. This is in accordance with most experimental reports on stoichiometric Fe_3Pd. Indeed, in the thermodynamic limit, Fe-Pd alloys in the MSM concentration range are expected to be unstable against decomposition into bcc-Fe and $L1_0$ FePd, which has also been confirmed by recent DFT ground-state calculations.[28] In contrast, Buschow *et al*. noted in their large survey of magneto-optical properties of more than 200 alloy compositions the appearance of order after long-time annealing.[71] Thus this issue must be considered unresolved from the experimental point of view and—although it appears unlikely judging from the total energy differences only—the appearance of partial and short-range order cannot be excluded entirely on the basis of the present results either.

Considerable static relaxations are indeed expected when different atomic radii are associated with the two atomic species (one 3*d* and one 4*d* element, in our case), which have indeed been found to contribute in similar magnitude to the total energy.[44] Significant static relaxations were also reported by Liot and collaborators for equiatomic $Fe_{50}Ni_{50}$[72] and from a recent 64-atom SQS calculation of an fcc $Fe_{65}Ni_{35}$ Invar alloy,[73] where the atomic radii of the 3*d* elements are of similar size. Here, the effect was attributed in part to different magnetic states of the atoms. Fe-Pd alloys exhibit in the Fe-rich composition range, similar to Fe-Ni and Fe-Pt, Invar-type anomalies, thus comparable mechanisms might be expected in Fe-Pd, too.

The major point of Fig. 2, however, lies in demonstrating that the energetic contribution from these displacements is not uniform and varies strongly across the binding surface, significantly increasing toward the bcc side. This has immediate consequences in the vicinity of phase transitions, if the binding surface is essentially flat. Thus, one must conclude—with respect to structural changes—that analytic descriptions of disorder which do not take care of static relaxations, as, for example, within the CPA, may not be appropriate for the prediction of ground-state structures in such cases. This would require the extension of the multiple scattering formalism in terms of a CPA taking into account the characteristic displacements of the atoms (on average).

A constant volume cross section of the binding surface of $Fe_{75}Pd_{25}$ from 108-atom supercell calculations is provided in Fig. 3. The energies are given relative to the disordered case at $c/a = 1$ (fcc) with atoms fixed at the ideal lattice positions. These are represented by triangles and diamonds and displayed in the upper part. Since, as mentioned above, the distribution of atoms in the supercell does not obey cubic symmetry, the binding curves differ depending on which of the Cartesian axes of the supercell is chosen to become the short *c* axis. The absolute difference for all three possibilities are of the order of 5 meV/atom along the complete Bain path. The discrepancy with respect to the *k* mesh is of similar magnitude. It appears largest close to the center of the Bain path.

The unrelaxed fcc cell has been used as the starting point for the structural optimization. Afterwards the Bain path was

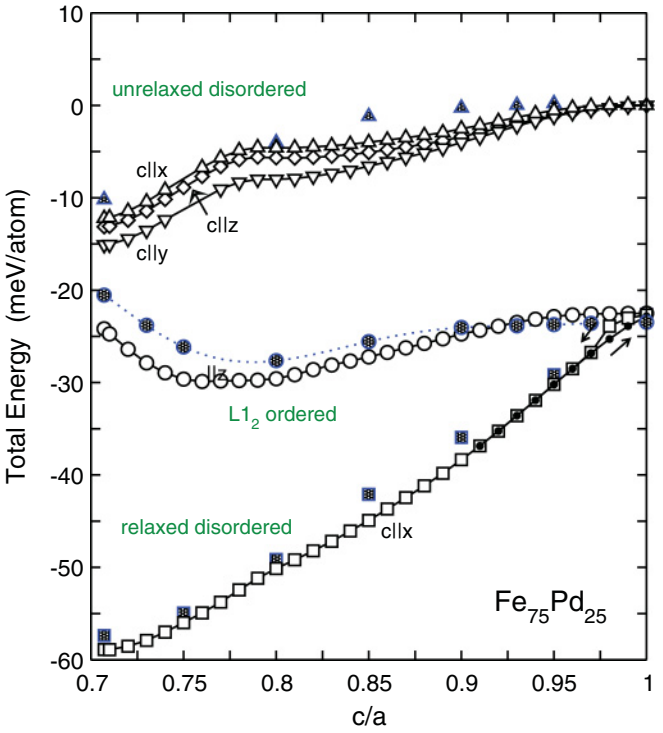

FIG. 3. (Color online) Total energy of relaxed and unrelaxed disordered and ordered structures of $Fe_{75}Pd_{25}$ along the Bain path. Reference for all curves is the disordered, unrelaxed fcc geometry at $c/a = 1$. Calculations with a mesh of $2\times2\times2$ *k* points are shown as open symbols (black), with a *k* mesh of $4\times4\times4$ as shaded symbols (blue). All calculations were carried out for the same atomic volume (13.08 Å^3/atom). For all but two calculations the shortened *c* axis has been chosen parallel to the *x* axis of the fcc supercell (upward triangles; symbols as in Fig. 2). For comparison the calculation of the unrelaxed disordered structure has been repeated with the *c* axis parallel to the *y* axis (downward triangles) and the *y* axis (diamonds). This shows that the error due to insufficient statistics is comparable to the error caused by a limited *k* mesh (≈5 meV/atom along the Bain path). The relaxed disordered configurations (open squares) have been obtained in consecutive relaxation and deformation steps starting from c/a=1 (as denoted by the arrows). Reversing this sequence (small solid circles) leads to a small region close to c/a=1 where the total energy depends on the deformation history.

sampled from the fcc to the bcc side, initializing the calculation for the next c/a value with the optimized configuration of the preceding one. An interesting detail in this respect is that reversing the sequence of alternating shear and relaxation steps, now approaching fcc starting from $c/a = 0.90$, leads to a small hysteresis which only appears in the vicinity of the cubic structure. This suggests that the potential energy surface will consist of a number of nearly degenerate local minima, which are capable of providing a kind of memory of previous deformations. A possible reason for this behavior will be discussed later in Sec. V. This dependence of the elastic response on the sample history might lead to problems in the precise determination of mechanical equilibrium properties as elastic constants, especially in the vicinity of the fcc structure. The effect on the total energy, however, is small and inferior to the other technical sources of errors, due to

the potentials, the incomplete convergence of the k mesh, and the spatially inhomogeneous distribution of the atomic species across the supercell. In total, these inaccuracies may add up to an uncertainty of the order of 10 meV/atom along the complete Bain path for the 108-atom system. This aspect should be kept in mind with respect to the absolute numbers provided by this work.

IV. BINDING SURFACE OF Fe-Pd MAGNETIC SHAPE-MEMORY ALLOYS

The stoichiometric composition provides firm grounds for a comparison with the ordered alloys, which are much easier to handle from the computational point of view. However, the technological interest is restricted mainly to compositions around $Fe_{70}Pd_{30}$. Therefore, additional calculations have been carried out for this and more Pd-rich compositions. Our results demonstrate that, in accordance with the experimental phase diagram, the fcc structure becomes increasingly favorable with decreasing Fe content. This trend is more pronounced for the unrelaxed, ideal lattice. Here the energy difference between fcc and bcc, $E_{\mathrm{bcc}}^{\mathrm{ideal}} - E_{\mathrm{fcc}}^{\mathrm{ideal}}$, increases from -10 meV/atom for $Fe_{75}Pd_{25}$ to $+6$ meV/atom in $Fe_{70.4}Pd_{29.6}$ as can be seen from the right panel of Fig. 4. In $Fe_{65.7}Pd_{34.3}$, a value of $+21$ meV/atom is reached. For the relaxed structures,

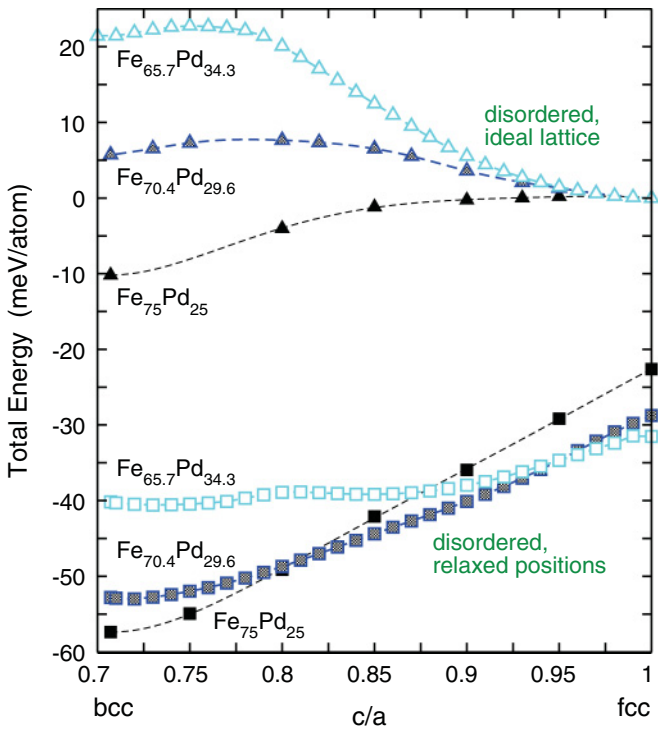

FIG. 4. (Color online) Total energy of relaxed (squares) and unrelaxed (triangles) disordered and ordered structures of $Fe_{75}Pd_{25}$, $Fe_{70.4}Pd_{29.6}$, and $Fe_{66}Pd_{34}$ along the Bain path (solid, shaded, and open symbols, respectively). Reference for each composition is the disordered, unrelaxed fcc geometry at $c/a = 1.0$. All calculations were carried out for the same atomic volume (13.08 Å^3/atom) with a k mesh of $4\times4\times4$ points in the irreducible Brillouin zone. The shortened c axis has been chosen parallel to the x axis of the fcc supercell. The lines are only a guide to the eye.

the change in binding energy, $E_{\mathrm{bcc}}^{\mathrm{relaxed}} - E_{\mathrm{fcc}}^{\mathrm{relaxed}}$, is decreasing accordingly from -35 meV/atom to -24 meV/atom for $Fe_{70.4}Pd_{29.6}$ and -8 meV/atom for $Fe_{65.7}Pd_{34.3}$, respectively. At the same time, the energy gain due to relaxation, $E_{\mathrm{fcc}}^{\mathrm{relaxed}} - E_{\mathrm{fcc}}^{\mathrm{ideal}}$, is increased (29 meV/atom for $Fe_{70.4}Pd_{29.6}$ compared to 23 meV/atom in the stoichiometric case).

The binding curves shown in Fig. 4 are obtained at a constant fixed volume of 13.08 Å^3/atom. This simplification is reasonable under the condition that the equilibrium atomic volume does not change along the Bain path, which is a prerequisite for a thermoelastic martensitic transformation which is a peculiar property of magnetic and conventional shape-memory alloys. Indeed, the complete binding surface of $Fe_{70.4}Pd_{29.6}$, which is shown in Fig. 5 (left), demonstrates that the relative variation of the equilibrium volume between the fcc state at $c/a = 1$ and the absolute minimum on the bcc side is of the order of $\Delta V/V = 0.75\%$. Although about one order of magnitude larger than for other shape-memory systems,[75] this value is still sufficiently small that the corresponding error does not impair the overall accuracy of the present calculations. Furthermore, the shape of the constant volume cross sections does not change significantly in the vicinity of the equilibrium volume. Nevertheless, since hydrostatic pressure is known to stabilize the martensitic phase, obtaining the full binding surface for all compositions is desirable for future high-precision investigations. Furthermore, a difference in the equilibrium volume between ordered and disordered configurations will influence the martensite stabilization by symmetry conforming aging processes involving short-range order or rearrangement of defects.[76,77]

The location of the absolute minimum appears shifted slightly toward larger c/a ratios, away from the ideal bcc value. This may be seen as a tentative indication that the ground state is, as found in experiment, a slightly tetragonally distorted bcc structure. But, again, the respective gain in energy is rather small compared to the technical uncertainties. Similar reasoning might hold true for the apparent tendency to form a double minima structure as indicated in the binding curve of $Fe_{65.7}Pd_{34.3}$ shown in Fig. 4. For more Fe-rich compositions, however, the variation upon tetragonal distortion along the Bain path can be regarded as rather smooth and monotonous and the binding surface does not exhibit clear features which may play a significant role at finite temperatures and can be related to the existence of an fct phase. Thus, one important question emerging from this observation is what—if not specific features of the binding surface—is the stabilizing origin of the fct structure, which is the relevant phase for MSM applications and found in experiment at finite temperatures.

Face-centered cubic Fe-Pd in the respective concentration range is known to exhibit Invar-like anomalies of the thermal expansion arising from a strong interaction between magnetic and spatial degrees of freedom. Thus in order to obtain a complete picture, the relation between magnetic properties and structural distortion also needs to be accounted for. Figure 5 shows that the ground-state spin magnetic moment depends solely on the volume per atom and is hardly changing along the Bain path. This is in nearly quantitative agreement with the extrapolation of the experimental saturation magnetization to $T = 0$ as shown in Fig. 6 and the concentration-dependent hyperfine field distribution obtained

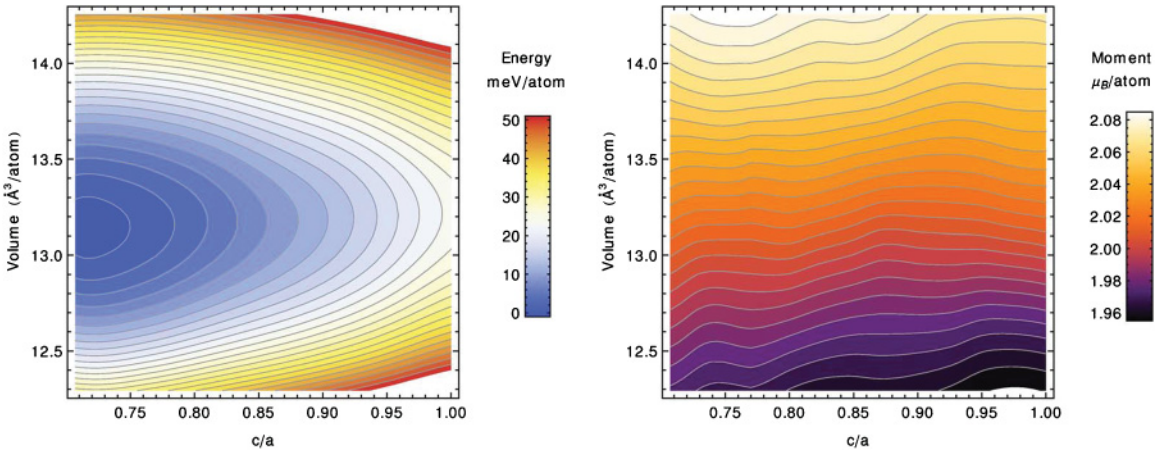

FIG. 5. (Color online) Complete binding surface $E(V,c/a)$ (left) and magnetization profile $M(V,c/a)$ (right) of the $Fe_{70.4}Pd_{29.6}$ alloy obtained by 108-atom supercell calculations including structural relaxations of the atoms ($4\times4\times4$ k points). The binding surface exhibits one single minimum close to bcc ($V_0 = 13.14$ Å/atom, $c/a = 0.717$) and no signature of an fct minimum at larger c/a. Ground-state magnetization (right panel) and equilibrium volume vary only slightly along the Bain path. Contour lines are drawn every 2 meV or 0.005 μ_B, respectively.

from Mößbauer experiments.[78] The average data arise from a stable high-spin Fe moment of 2.72 μ_B and an induced Pd moment of 0.31 μ_B at the fcc end. While the former hardly varies along the Bain path (slightly reduced by approximately 0.01 μ_B for bcc), the Pd moments increase steadily upon tetragonal distortion reaching a value of about 0.35 μ_B on the bcc side, consequently leading to a slightly enhanced total moment, here, in agreement with the experimental trend.

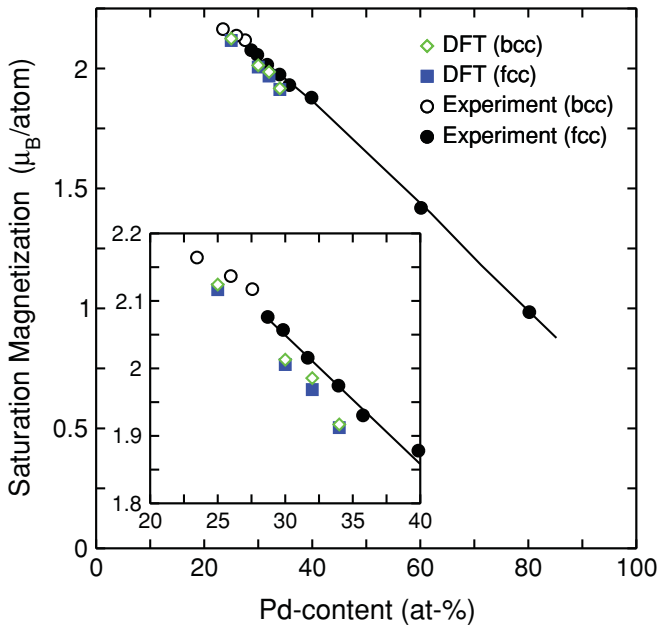

FIG. 6. (Color online) (Left) Comparison of the calculated magnetization (average spin moment per atom) with experimental data extrapolated to $T = 0$ obtained from Ref. 74. Since the DFT calculations do only consider the spin moments and neglect orbital contributions, the values are consequently a few hundreds of μ_B smaller than in experiment. The theoretical values for the bcc structures are slightly larger than for fcc coordination. This trend corresponds to the small jump in the experimental data at the fcc-bcc transition.

Furthermore, the static distortions do not contribute significantly to the magnetic properties. If the atoms are located on ideal lattice positions, the average magnetic moment increases only slightly by 1%–2%, regardless of the tetragonal distortion of the lattice. Thus, judging from the present calculations, there is no trace of a considerable interdependence between magnetism and structure at $T = 0$. Nevertheless, although not visible in our ground-state calculations, Invar-type excitations will be present at finite temperatures especially on the fcc side and it can be speculated whether they might provide a further contribution to the free energy stabilizing the cubic and eventually also the fct phase.

V. ELECTRONIC ORIGIN OF THE STATIC DISPLACEMENTS

The previous section has shown that static ionic displacements have the potential to invert the energetic sequence of phases. Therefore, it is worthwhile to look at the origin of these local distortions in more detail. As the investigation of Opahle *et al.* has demonstrated,[52] Fe-rich Fe-Pd bears the prerequisites to exhibit a cubic-to-tetragonal instability according to a band-Jahn-Teller mechanism, arising from an enhanced electronic density of states (DOS) at the Fermi level. On the other hand, for the $L1_2$ ordered Fe_3Pd alloy, atomic relaxations lead to an antiferrodistortive displacement pattern, which only affects the Fe species. This arises from significant nesting portions of the Fe bands at the Fermi surface, which are connected by a k vector of (1/2,1/2,0), which exactly corresponds to the wave vector of a soft phonon in the transversal acoustic TA_1 branch,[30] as previously discussed in Sec. I. For the ordered Fe_3Pt alloy, this anomaly is well known from neutron diffraction experiments.[79–81] The ordered $L1_2$ structure can be conceived as corner-sharing Fe octahedra embedded in a simple cubic Pd matrix. The antiferrodistortive transformation breaks the cubic symmetry. This process results in a tetragonal lattice, which can be characterized by a pure Fe plane sandwiched between mixed Fe-Pd planes. The atoms in the mixed planes stay in place, while the atoms in

the Fe planes are subject to in-plane motion, which points inward and outward of the simple cubic lattice spanned by the stationary Pd atoms. In order to fulfill this constraint, the deformation pattern is rotated by 90% in adjacent cells in the x-y plane, which shows up as a short-wavelength modulation. This process invokes an orthorhombic distortion of the Fe octahedra, yielding a threefold splitting of the nearest neighbor Fe-Fe pair distances reminding one of the original Jahn-Teller picture.

A smeared out softening of the TA_1 branch in [110] direction has also been observed experimentally in disordered Fe-Pd and Fe-Pt alloys at smaller wave vectors away from the zone boundary.[81,82] Considering that Fe clusters, which are susceptible to this kind of distortion can be considered to be statistically distributed within the bulk alloy, this would finally result in a rather smeared out feature. It may be speculated whether this anomaly can be interpreted in terms of a corresponding distortion with similar electronic origin, occurring with a larger, statistically modified period.

Local distortions can be studied in a complementary way in terms of the radial pair distribution function $g(\mathbf{r}_i - \mathbf{r}_j)$, which is a measure of the conditional probability starting from lattice site i to find another atom at site j at the distance $r = |\mathbf{r}_i - \mathbf{r}_j|$:

$$g(r) = \sum_{i,j} \frac{\delta(r - |\mathbf{r}_i - \mathbf{r}_j|)}{4\pi r^2 \rho}, \quad (1)$$

where ρ is a normalizing factor representing the atomic density. To improve the presentation, the δ functions have been replaced by a Gaussian distribution function with a variance of 0.01 Å^2.

Jahn-Teller-like orthorhombic distortions of Fe octahedra show up in a threefold splitting of the nearest neighbor peak of the partial Fe-Fe distribution function $g_{\mathrm{Fe-Fe}}(r)$. In a previous attempt, this has been evaluated employing a disordered 108-atom supercell as in the present study.[83] Indeed, a considerable broadening of the nearest neighbor peak of $g_{\mathrm{Fe-Fe}}(r)$ is found. Its width is consistent with the spreading of the peak observed in the ordered alloy, but a clear proof for a threefold splitting is missing. One likely reason is that a 108-atom supercell does not provide sufficient statistics to resolve the fine features of $g(r)$. It may also be too small to accommodate longer-ranged elastic interactions mediated by the lattice strain fields, which may wash out characteristic distortion patterns. Therefore, the structural optimization procedure was repeated with the VASP code within a 500-atom $5\times5\times5$ sc supercell containing 160 Pd and 340 Fe atoms, yielding the nominal composition $Fe_{68}Pd_{32}$. The corresponding total and partial pair distribution functions, shown in Fig. 7, confirm that the nearest neighbor Fe-Fe peak is significantly wider compared to the mixed Fe-Pd as well as to the Pd-Pd peak. More important, a threefold splitting of the order of 0.05 Å, which is slightly smaller than the splitting predicted for the ordered alloy, is clearly visible. This indicates that also in the disordered alloy, structural anomalies are present, which arise solely from interactions between Fe pairs. Keeping in mind the analogy to the Jahn-Teller distorted octahedra in ordered Fe_3Pd, it is straightforward to conceive that the actual relaxation patterns of corresponding Fe clusters in the disordered alloy will likely accommodate a tetragonal distortion of the lattice by changing their relative orientation.

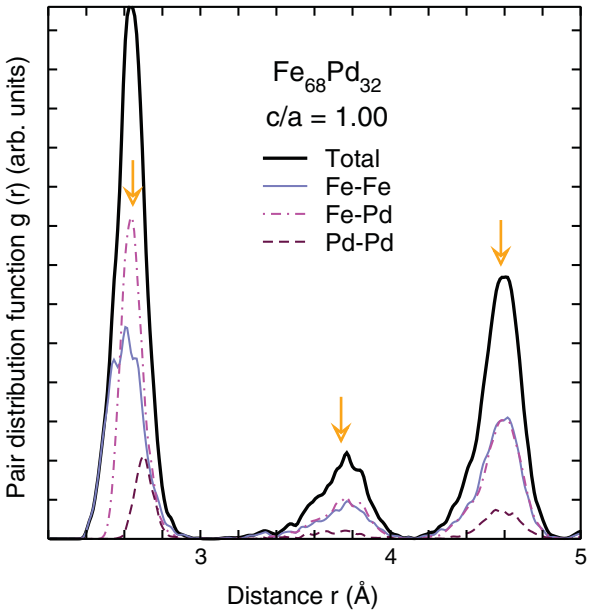

FIG. 7. (Color online) Total and partial radial pair distribution function $g(r)$ of a 500-atom $Fe_{68}Pd_{32}$ supercell describing a disordered fcc alloy obtained after *ab initio* structure optimization. The thick black line refers to the total pair correlation function $g(r)$, while the thinner solid (blue), dashed (brown), and dash-dotted (magenta) lines refer to the partial contributions arising from pure Fe pairs, Pd pairs, and mixed Fe-Pd pairs, respectively. The arrows (orange) mark the positions of the ideal lattice peaks.

The consequence is a kind of memory of the sample history, eventually showing up in a small hysteresis as the one observed in Fig. 3.

The Fe-Fe contribution marks the left end, while $g_{\mathrm{Fe-Pd}}(r)$ and $g_{\mathrm{Pd-Pd}}(r)$ peak at the center and at the right end of the first peak in the total $g(r)$. This, in turn, is owed to the different atomic radii of the elements and reflected in the large spread of 0.1 Å in the element-resolved average nearest neighbor distances, which are given together with the corresponding values for next-nearest and third neighbors in Table I. The second and third peaks are significantly broader than the first one while the spread between the average contributions has become significantly smaller. In contrast to the nearest neighbor case, where the Pd-Pd pairs experience the largest separation, they are now found at closer distances than the

TABLE I. Averages of the element-resolved neighbor distances $r = |\mathbf{r}_i - \mathbf{r}_j|$ between nearest, next-nearest, and third-nearest neighbor pairs and the corresponding spacing for the ideal fcc lattice with the same lattice constant. The numbers in parentheses are the corresponding standard deviations. The average displacements from the initial ideal lattice positions are 0.1764 Å (± 0.0730Å) for Fe and 0.1707 Å (± 0.0688Å) for Pd.

$\bar{r}$ (Å)	Nearest	Next nearest	Third nearest
Fe-Fe	2.626(0.092)	3.739(0.165)	4.581(0.112)
Fe-Pd	2.657(0.059)	3.755(0.126)	4.587(0.107)
Pd-Pd	2.717(0.049)	3.708(0.151)	4.593(0.099)
Ideal	2.645	3.740	4.581

Fe pairs, which are on average one lattice constant apart from each other; only the mixed contribution reflects the larger size of the Pd atoms. Interestingly, although the Pd-Pd distances experience in both cases the largest deviations from the pair distances of the ideal lattice, the average absolute shift of the atoms with respect to their ideal lattice positions is (slightly) larger for the Fe species. For the third neighbor peak, differences between the partial contributions are not encountered and all partial contributions match the shape of the total $g(r)$. This indicates that the most important interactions are presumably between nearest neighbor pairs and the size effect averages out at longer distances. However, in particular the second neighbor peak is rather asymmetric, extending toward smaller distances. During the transformation along the Bain path from fcc to bcc first and second neighbor peaks split up. Fractions of both, four atoms of the first and two of the second neighbor peak, move closer to each other and finally join to form the second neighbor peak of the bcc lattice. Thus, this feature might be interpreted as a precursor for the onset of a tetragonal distortion, which arises from the interatomic interactions and is already present in the displacement pattern of the cubic phase.

The static distortions can be related to changes in the electronic DOS. The DOS is evaluated with a mesh of $4\times4\times4$ k points since it is more susceptible to the convergence with respect to the k mesh than the structural quantities. This allows the interpretation of fine features giving rise to a band-Jahn-Teller mechanism. A comparison of the DOS with respect to changes arising from local lattice distortions is shown in Fig. 8. Indeed, the minority DOS corresponding to the unrelaxed configuration exhibits a tiny but noticeable maximum just below the Fermi level, which moves to lower energies after optimization, while the Fermi level comes to lie in a local minimum. Indeed, only Fe states contribute to this peak and significant changes of the Pd partial contributions—apart from a hardly visible shift of a hybridization hump close to E_{Fermi}—are not present after relaxation. This substantiates that the threefold multimodal splitting of the $g_{\mathrm{Fe-Fe}}(r)$ is largely independent of the interactions with the surrounding Pd atoms.

Further differences in the Fe partial DOS, which might be responsible for the comparatively large changes of the total energy, are encountered in the majority spin channel, where the typical fcc-type three-peak structure extending from -0.5 eV down to -3.5 eV is washed out to a large extent. This again has only minor effect on the Pd DOS, which is rather flat below -1 eV. Significant changes in the Pd DOS, however, are found at the lower edge of the d band, in analogy to reports on the disordered $Cu_{75}Pd_{25}$ alloy.[44] The bandwidth of 4d metals is naturally larger than for 3d metals and thus the Pd 4d electrons dominate the lower edge of the d band, while 3d-4d hybridization drags Fe states down. During relaxation, the width of the d band decreases. This is owed to the increased distance between the Pd atoms in the relaxed structures with respect to the overall average value, as can be seen in Fig. 7. The relaxation of the Pd atoms should be expected to be larger on the bcc side, since it is the more open structure, potentially providing a larger contribution to the total energy. According to this interpretation, the relaxations are emerging to the partial electronic pressure of the 4d electrons and only a fraction can be accounted for by the band-Jahn-Teller mechanism which is only present on the fcc side and largely independent of the other mechanism.

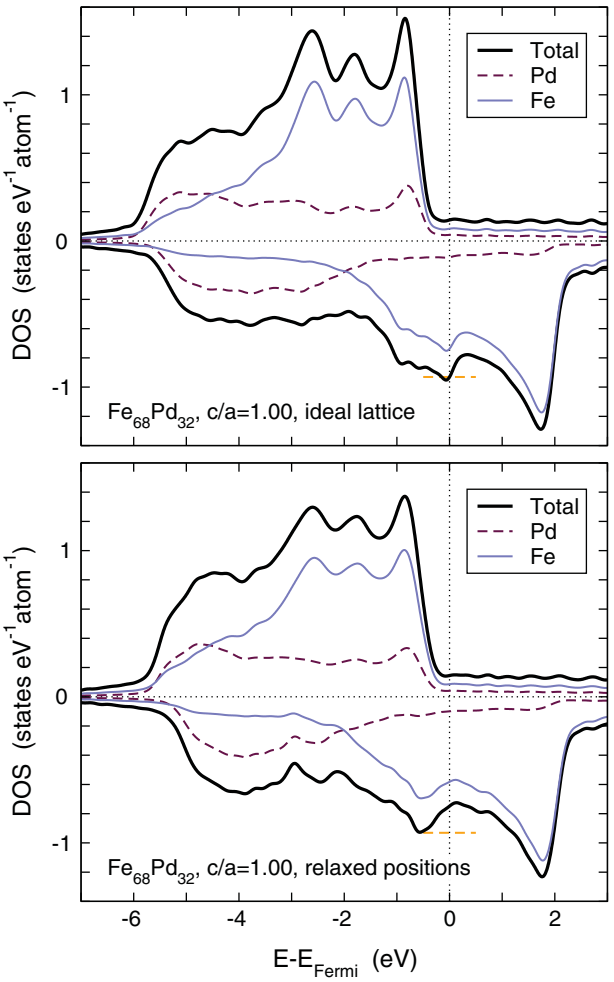

FIG. 8. (Color online) Electronic density of states of the disordered $Fe_{68}Pd_{32}$ alloy obtained from a 500-atom supercell calculation. (Top) Face-centered cubic structure ($c/a = 1$) with atoms on ideal positions. (Bottom) DOS after structural relaxation. The total DOS are represented by the thick black lines; thinner blue and brown lines refer to partial Fe and Pd contributions, respectively. For better comparison, the minority DOS at the Fermi level of the unrelaxed disordered fcc configuration is marked in both panels by a broken horizontal line (orange color).

VI. CONCLUSIONS

We explored the binding surface, ordering, and compositional tendencies of martensitically transforming Fe-rich Fe-Pd alloys, which are in the compositional range of interest for magnetic shape-memory applications and Invar-type thermal expansion anomalies, by means of first-principles calculations obtained within a 108-atom supercell including unconstrained optimization of atomic positions. It was demonstrated that the energetic contribution of atomic relaxations varies significantly upon a tetragonal distortion along the Bain path, which connects face-centered and body-centered cubic structures. Close to the $Fe_{70}Pd_{30}$ magnetic shape-memory

composition, this leads to a qualitative change of structural properties, manifesting in an inversion of slope and curvature of the binding surface, which makes the fcc austenite unstable against a tetragonal distortion. Naturally, this can only occur in the vicinity of the martensitic phase transformation since only here the binding surface is sufficiently flat and local distortions and corresponding lattice vibrations may contribute significantly to the free energy surface. Although the ground-state calculations do not predict a significant variation of the magnetic structure along the Bain path, finite temperature magnetic excitations should be taken into account as well in further investigations.

By means of large-scale calculations involving a 500-atom $Fe_{68}Pd_{32}$ supercell, we identified in accordance with a previous study based on an analytic description of disorder[52] an accumulation of Fe states at the Fermi level for the ideal, undistorted lattice, which potentially gives rise to a band-Jahn-Teller relaxation mechanism. The optimization of atomic positions, which is possible within the supercell approach, reveals that a tetragonal distortion which can resolve this potentially unstable situation will be in close competition with corresponding changes in local atomic arrangement. From the statistical mechanics point of view it appears likely that uncorrelated local processes will dominate over a collective distortion. As a consequence the local Jahn-Teller-type distortions could set up a preference for a tetragonal distortion of the lattice. This is the case for the highly ordered Fe_3Pt alloy[30,84] and indicated by the asymmetric shape of the second neighbor peak in the pair distribution function in the present study. However, the fact that the Jahn-Teller mechanism in Fe-Pd is superimposed by distortions related to the different atomic sizes, which cannot be disregarded in the Fe-Pd system impedes the substantiation of this conjecture on the basis of the present data.

ACKNOWLEDGMENTS

The authors gratefully acknowledge helpful discussions with Sandra Weiß, Sebastian Fähler (Dresden), Sven Hamann, Alfred Ludwig (Bochum), Jan Minár (München), Mehmet Acet, and Eberhard Wassermann (Duisburg-Essen). Substantial parts of the calculations were carried out on the JUGENE supercomputer of the John von Neumann Institute for Computing, Forschungszentrum Jülich, and the Cray XT6m at University of Duisburg-Essen. The authors thank the John von Neumann Institute for Computing (NIC), Jülich Supercomputing Center (JSC), both of Forschungszentrum Jülich, as well as the Center for Computational Sciences and Simulation (CCSS) of the University of Duisburg-Essen for computing time and support. Financial support was granted by the Deutsche Forschungsgemeinschaft as part of the priority program SPP 1239, "Change of microstructure and shape of solid materials by external magnetic fields," within subproject C10, "Ab initio evaluation of phase stability, magnetism and twin boundary mobility in ternary Fe-based shape-memory materials."

*markus.gruner@uni-due.de

[1] M. Acet, L. Mañosa, and A. Planes, in *Handbook of Magnetic Materials*, Vol. 19 (Elsevier, Amsterdam, 2011), Chap. 4, p. 231.
[2] V. A. Chernenko and V. A. L'vov, Mater. Sci. Forum **583**, 1 (2008).
[3] P. Entel, V. D. Buchelnikov, V. V. Khovailo, A. T. Zayak, W. A. Adeagbo, M. E. Gruner, H. C. Herper, and E. F. Wassermann, J. Phys. D: Appl. Phys. **39**, 865 (2006).
[4] Z. Nishiyama, *Martensitic Transformation* (Academic Press, New York, 1978).
[5] W. Pepperhoff and M. Acet, in *Engineering Materials*, Vol. VIII (Springer, Berlin, 2001).
[6] E. F. Wassermann and M. Acet, in *Magnetism and Structure in Functional Materials*, edited by A. Planes, L. Manõsa, and A. Saxena (Springer, Berlin, 2005), Vol. 79 of Springer Series in Materials Science, p. 177.
[7] C.-E. Guillaume, C. R. Acad. Sci. (Paris) **125**, 235 (1897).
[8] E. F. Wassermann, in *Ferromagnetic Materials*, edited by K. H. J. Buschow and E. P. Wohlfahrt (Elsevier, Amsterdam, 1990), Vol. 5, Chap. 3, p. 237.
[9] M. Shiga, in *Materials Science and Technology*, edited by R. W. Cahn, P. Haasen, and E. J. Kramer (VCH, Weinheim, 1994), Vol. 3B, Chap. 10, p. 159.
[10] M. Matsui, H. Yamada, and K. Adachi, J. Phys. Soc. Jpn. **48**, 2161 (1980).
[11] S. Muto, R. Oshima, and F. E. Fujita, Metall. Trans. A **19**, 2723 (1988).
[12] J. Cui, T. W. Shield, and R. D. James, Acta Mater. **52**, 35 (2004).
[13] T. Kakeshita and T. Fukuda, Mater. Sci. Forum **394-395**, 531 (2002).
[14] T. Fukuda, T. Sakamoto, T. Kakeshita, T. Takeuchi, and K. Kishio, Mater. Trans. **45**, 188 (2004).
[15] T. Kakeshita, T. Fukuda, and T. Takeuchi, Mater. Sci. Eng. A **438-440**, 12 (2006).
[16] R. Hayashi, S. Murray, M. Marioni, S. Allen, and R. O'Handley, Sensors and Actuators **81**, 219 (2000).
[17] D. Vokoun, Y. W. Wang, T. Goryczka, and C. T. Hu, Smart Mater. Struct. **14**, S261 (2005).
[18] S. Hamann, A. Savan, S. Thienhaus, and A. Ludwig, in *ACTUATOR 2008, 11th International Conference on New Actuators* (Bremen, Germany, 2008), p. 271.
[19] V. Sánchez-Alarcos, V. Recarte, J. Pérez-Landazábal, M. GonzÍez, and J. Rodríguez-Velamazán, Acta Mater. **57**, 4224 (2009).
[20] S. Hamann, M. E. Gruner, S. Irsen, J. Buschbeck, C. Bechtold, I. Kock, S. G. Mayr, A. Savan, S. Thienhaus, E. Quandt, S. Fähler, P. Entel, and A. Ludwig, Acta Mater. **58**, 5949 (2010).
[21] K. Ullakko, J. K. Huang, C. Kantner, R. C. O'Handley, and V. V. Kokorin, Appl. Phys. Lett. **69**, 1966 (1996).
[22] A. Sozinov, A. A. Likhachev, N. Lanska, and K. Ullakko, Appl. Phys. Lett. **80**, 1746 (2002).
[23] O. Söderberg, Y. Ge, A. Sozinov, S.-P. Hannula, and V. V. Lindroos, Smart Mater. Struct. **14**, 223 (2005).
[24] V. A. Chernenko, C. Segui, E. Cesari, J. Pons, and V. V. Kokorin, Phys. Rev. B **57**, 2659 (1998).
[25] V. V. Khovaylo, V. D. Buchelnikov, R. Kainuma, V. V. Koledov, M. Ohtsuka, V. G. Shavrov, T. Takagi, S. V. Taskaev, and A. N. Vasiliev, Phys. Rev. B **72**, 224408 (2005).

[26]M. Richard, J. Feuchtwanger, D. Schlagel, T. Lograsso, S. Allen, and R. O'Handley, Scr. Mater. **54**, 1797 (2006).
[27]E. C. Bain, Trans. Am. Inst. Min. Metall. Eng. **70**, 25 (1924).
[28]S. V. Barabash, R. V. Chepulskii, V. Blum, and A. Zunger, Phys. Rev. B **80**, 220201 (2009).
[29]T. Yamamoto, M. Yamamoto, T. Fukuda, T. Kakeshita, and H. Akai, Mater. Trans. **51**, 896 (2010).
[30]M. E. Gruner, W. A. Adeagbo, A. T. Zayak, A. Hucht, and P. Entel, Phys. Rev. B **81**, 064109 (2010).
[31]M. Podgórny, Phys. Rev. B **43**, 11300 (1991).
[32]P. Entel, E. Hoffmann, P. Mohn, K. Schwarz, and V. L. Moruzzi, Phys. Rev. B **47**, 8706 (1993).
[33]V. N. Antonov, B. N. Harmon, and A. N. Yaresko, Phys. Rev. B **64**, 024402 (2001).
[34]Y. Chen, T. Atago, and T. Mohri, J. Phys. Condens. Matter **14**, 1903 (2002).
[35]Z. Major, S. B. Dugdale, T. Jarlborg, E. Bruno, B. Ginatempo, J. B. Staunton, and J. Poulter, J. Phys. Condens. Matter **15**, 3619 (2003).
[36]V. L. Moruzzi, Physica B **161**, 99 (1989).
[37]V. L. Moruzzi, Phys. Rev. B **41**, 6939 (1990).
[38]D. D. Johnson, F. J. Pinski, J. B. Staunton, G. M. Stocks, and B. L. Györffy, in *Physical Metallurgy of Controlled Expansion Invar-Type Alloys*, edited by K. C. Russel and D. F. Smith (The Minerals Metals & Materials Society, Warrendale, 1990), p. 3.
[39]M. Schröter, H. Ebert, H. Akai, P. Entel, E. Hoffmann, and G. G. Reddy, Phys. Rev. B **52**, 188 (1995).
[40]S. Khmelevskyi, I. Turek, and P. Mohn, Phys. Rev. Lett. **91**, 037201 (2003).
[41]S. Khmelevskyi and P. Mohn, Phys. Rev. B **69**, 140404 (2004).
[42]A. Ruban and I. Abrikosov, Rep. Prog. Phys. **71**, 046501 (2008).
[43]A. Zunger, S.-H. Wei, L. G. Ferreira, and J. E. Bernard, Phys. Rev. Lett. **65**, 353 (1990).
[44]Z. W. Lu, S.-H. Wei, and A. Zunger, Phys. Rev. B **45**, 10314 (1992).
[45]D. Shin, A. van de Walle, Y. Wang, and Z.-K. Liu, Phys. Rev. B **76**, 144204 (2007).
[46]K. Tarafder, S. Ghosh, B. Sayal, O. Eriksson, A. Mookerjee, and A. Chakrabarti, J. Phys. Condens. Matter **20**, 445201 (2008).
[47]G. Ghosh, A. van de Walle, and M. Asta, Acta Mater. **56**, 3202 (2008).
[48]J. von Pezold, A. Dick, M. Friák, and J. Neugebauer, Phys. Rev. B **81**, 094203 (2010).
[49]R. A. Stern, S. D. Willoughby, A. Ramirez, J. M. MacLaren, J. Cui, Q. Pan, and R. D. James, J. Appl. Phys. **91**, 7818 (2002).
[50]R. A. Stern, S. D. Willoughby, J. M. MacLaren, J. Cui, Q. Pan, and R. D. James, J. Appl. Phys. **93**, 8644 (2003).
[51]E. Burzo and P. Vlaic, J. Optoelectron. Adv. Mater. **12**, 1869 (2010).
[52]I. Opahle, K. Koepernik, U. Nitzsche, and M. Richter, Appl. Phys. Lett. **94**, 072508 (2009).
[53]K. Koepernik and H. Eschrig, Phys. Rev. B **59**, 1743 (1999).
[54]H. Eschrig, M. Richter, and I. Opahle, in *Relativistic Electronic Structure Theory, Part II. Applications*, edited by P. Schwerdtfeger (Elsevier, Amsterdam, 2004), Vol. 14 of *Theoretical and Computational Chemistry*, p. 723.
[55][http://www.fplo.de].
[56]J. Buschbeck, I. Opahle, M. Richter, U. K. Rößler, P. Klaer, M. Kallmayer, H. J. Elmers, G. Jakob, L. Schultz, and S. Fähler, Phys. Rev. Lett. **103**, 216101 (2009).
[57]P. Blaha, K. Schwarz, G. K. H. Madsen, D. Kvasnicka, and J. Luitz, computer code WIEN2K (an augmented plane wave + local orbitals program for calculating crystal properties), Technische Universität Wien, Austria, 2001.
[58]P. Hohenberg and W. Kohn, Phys. Rev. **136**, B864 (1964).
[59]G. Kresse and J. Furthmüller, Phys. Rev. B **54**, 11169 (1996).
[60]M. E. Gruner and P. Entel, J. Phys. Condens. Matter **21**, 293201 (2009).
[61]G. Kresse and D. Joubert, Phys. Rev. B **59**, 1758 (1999).
[62]J. P. Perdew, in *Electronic Structure of Solids '91*, edited by P. Ziesche and H. Eschrig (Akademie Verlag, Berlin, 1991).
[63]J. P. Perdew, K. Burke, and Y. Wang, Phys. Rev. B **54**, 16533 (1996).
[64]S. H. Vosko, L. Wilk, and M. Nusair, Can. J. Phys. **58**, 1200 (1980).
[65]H. J. Monkhorst and J. D. Pack, Phys. Rev. B **13**, 5188 (1976).
[66]M. Methfessel and A. T. Paxton, Phys. Rev. B **40**, 3616 (1989).
[67]P. E. Blöchl, O. Jepsen, and O. K. Andersen, Phys. Rev. B **49**, 16223 (1994).
[68]H. Ebert *et al.*, computer code SPR-KKR (the Munich SPR-KKR package, version 5.4) [http://olymp.cup.uni-muenchen.de/ak/ebert/SPRKKR].
[69]H. Ebert, in *Electronic Structure and Physical Properties of Solids*, edited by H. Dreyssé (Springer, Berlin, 2000), vol. 535 of Lecture Notes in Physics, p. 191.
[70]J. P. Perdew, K. Burke, and M. Ernzerhof, Phys. Rev. Lett. **77**, 3865 (1996).
[71]K. H. J. Buschow, P. G. van Engen, and R. Jongebreur, J. Magn. Magn. Mater. **38**, 1 (1983).
[72]F. Liot, S. Simak, and I. Abrikosov, J. Appl. Phys. **99**, 08P906 (2006).
[73]F. Liot and I. A. Abrikosov, Phys. Rev. B **79**, 014202 (2009).
[74]M. Matsui, T. Shimizu, H. Yamada, and K. Adachi, J. Magn. Magn. Mater. **15-18**, 1201 (1980).
[75]V. A. Chernenko and V. A. L'vov, Philos. Mag. A **73**, 999 (1996).
[76]X. Ren and K. Otsuka, Nature (London) **389**, 579 (1997).
[77]V. A. L'vov, A. Kosgor, O. Söderberg, and S.-P. Hannula, Mater. Sci. Forum **635**, 13 (2010).
[78]S. Klimars, J. Hesse, and B. Huck, J. Magn. Magn. Mater. **51**, 183 (1985).
[79]Y. Noda and Y. Endoh, J. Phys. Soc. Jpn. **57**, 4225 (1988).
[80]J. Kästner, W. Petry, S. Shapiro, A. Zheludev, J. Neuhaus, T. Roessel, E. Wassermann, and H. Bach, Eur. Phys. J. B **10**, 641 (1999).
[81]J. Kästner, J. Neuhaus, E. Wassermann, W. Petry, B. Hennion, and H. Bach, Eur. Phys. J. B **11**, 75 (1999).
[82]M. Sato, B. H. Grier, S. M. Shapiro, and H. Miyajima, J. Phys. F **12**, 2117 (1982).
[83]M. E. Gruner, MRS Proceedings **1200**, 1200-G04-04 (2009).
[84]M. Yamamoto, T. Fukuda, T. Kakeshita, K. Koyama, and N. Nojiri, Physics Procedia **10**, 117 (2010).